*applied sciences*

MDPI

*Article*

# Cell Concentration Modulates Pulsed Electric Fields' Bioeffects: Integrated Electrical, Viability, and Metabolic Analysis

**Viviana M. Caldeira [1,*], Cecília R. C. Calado [1] and Luis M. S. Redondo [2,3]**

[1] Research & Development Laboratory in Health and Engineering, ISEL-Instituto Superior de Engenharia de Lisboa, Instituto Politécnico de Lisboa, Rua Conselheiro Emídio Navarro 1, 1959-007 Lisbon, Portugal; cecilia.calado@isel.pt

[2] Pulsed Power Advanced Applications Group (GIAAPP), ISEL-Instituto Superior de Engenharia de Lisboa, Instituto Politécnico de Lisboa, Rua Conselheiro Emídio Navarro 1, 1959-007 Lisbon, Portugal; luis.redondo@isel.pt

[3] EnergyPulse Systems (EPS), Lispolis, 1600-546 Lisbon, Portugal

* Correspondence: vcaldeira.research@gmail.com

### Featured Application

Criteria for selecting cell concentrations in pulsed electric field (PEF) protocols, based on the effects on current, Joule heating, and post-PEF recovery.

### Abstract

Pulsed electric field (PEF) technology shows great promise for non-thermal biomedical applications, including gene electrotransfer and tissue engineering. However, the influence of cell concentration and density on the electrical and biological responses to PEFs remains insufficiently characterized. This study evaluated the association between cell concentration, electrical response, viability, post-treatment recovery, and FTIR spectral profiles following microsecond PEF exposure. L929 fibroblasts were exposed to a fixed protocol of 10 kV/cm, with five 5 µs pulses at 1 Hz, using five concentrations ranging from $5.0 \times 10^4$ to $1.0 \times 10^6$ cells in 0.8 mL of DPBS. Higher cell concentrations were associated with lower peak current and temperature increases, with the peak current decreasing from 429 A at $5.0 \times 10^4$ cells to 269 A at $1.0 \times 10^6$ cells and the maximum temperature decreasing from 12.8 to 8.0 °C. Immediate post-PEF viability was lower at the two lowest concentrations, whereas all groups showed substantial recovery after 72 h, with viability ranging from 73.5% to 98.0%. FTIR and principal component analysis identified treatment-associated changes in spectral profiles, followed by partial convergence toward the non-PEF condition after recovery. These findings indicate that cell concentration is an important process parameter in this experimental PEF model, with direct implications for scaling biomedical PEF applications and tissue engineering protocols.

**Keywords:** pulsed electric fields; electroporation; cell concentration; FTIR spectroscopy; metabolomics

Check for updates

Academic Editor: Claude Verdier

Received: 29 June 2026
Revised: 7 August 2026
Accepted: 16 October 2026
Published: 26 October 2026

**Copyright:** © 2026 by the authors. Licensee MDPI, Basel, Switzerland. This article is an open access article distributed under the terms and conditions of the Creative Commons Attribution (CC BY) license.

## 1. Introduction

Pulsed electric field (PEF) technology is a way of manipulating the cell plasma membrane and its internal components and functions with reduced thermal load. In mammalian cells, PEFs can trigger diverse biological processes, including activation of signaling pathways and membrane permeabilization. Electroporation is the phenomenon that results from exposing biological phospholipid bilayers to an external electric field of sufficient

intensity and increases their permeability, i.e., the formation of pores in the cell membrane, allowing the redistribution of electrical charges on both sides of the phospholipid bilayer. In this way, water molecules penetrate this bilayer, forming a "water wire" that induces phospholipid reorganization and shifts the hydrophilic head toward the water molecules, thereby forming stable channels or pores for ion passage [1]. The final biological effect depends on the number and type of targeted cells and on the PEF conditions, which can be precisely tuned to achieve reversible membrane permeabilization or irreversible cell death, spanning applications from industrial food processing, where PEFs are widely used, to biomedical gene therapy.

In food processing, pulsed electric fields (PEFs) have emerged as an innovative non-thermal technology capable of enhancing mass transfer in plant tissues and liquid matrices. By inducing electroporation in densely structured materials, PEF treatments reduce thermal degradation and increase extraction yields in processes such as juice recovery, oil extraction, and winemaking [2].

In recent years, PEFs have attracted considerable attention for their potential in biomedical research. Gene electrotransfer and electrochemotherapy are now regarded as promising therapeutic tools. Gene electrotransfer (GET) employs reversible electroporation to induce membrane permeabilization, electrophoretic DNA transport, and intracellular translocation, thereby improving transfection efficiency, a crucial step in vaccine development and gene therapy [3]. CRISPR/Cas9 is a promising gene-editing technology; however, despite its efficacy in many cancer cell lines, it is significantly less effective in more complex cell types, particularly primary cells, which are generally harder to transfect. Electroporation is a strategy to enhance CRISPR/Cas9 delivery, as it permeabilizes the nuclear membrane and enables efficient introduction of complexes into cell lines and primary cells that are resistant to routine chemical-based transfection methods [4]. PEFs are also used in irreversible electroporation (IRE), a non-thermal ablation technique for tumor treatment that employs high-voltage pulses to induce irreversible membrane permeabilization and cancer cell death, with field thresholds that ensure precise, localized, conductivity-dependent targeting [5]. Among therapeutic technologies, electrochemotherapy (ECT) remains the most established electroporation-based approach. By enhancing intracellular uptake of otherwise poorly permeable chemotherapeutics, ECT improves tumor specificity and reduces systemic toxicity in complex tissues [6]. Electroporation is also favorable for the valorization of platelet concentrates without transfusion. Platelets, which contain platelet-derived growth factor (PDGF), insulin-like growth factor (IGF), and transforming growth factor (TGF), are useful for tissue regeneration [7].

Optimized waveform parameters for PEF treatments depend on pulse duration, polarity, and waveform shape. During sample pulsing, changes in conductivity can lead to significant variations in delivered energy, requiring power modulators capable of sustaining the desired field amplitude across different scenarios. Although protocols optimized at laboratory scale are often successful, translating them into continuous systems remains challenging when accounting for higher cell densities and variable field distributions [8]. This is also challenging in bioprocessing applications, where it is necessary to operate at cell concentrations of $1.0 \times 10^8$ to $1.0 \times 10^9$ cells/mL, for example, in microalgae cultivation and platelet-rich plasma activation. PEFs are used in such systems to selectively modulate intracellular pathways rather than to completely disrupt cells. Variations in pulse strength and duration can modulate the release of growth factors such as PDGF, but sample conductivity and concentration strongly influence reproducibility [9]. Cell density alters electroporation through changes in conductivity, field inhomogeneity arising from cell polarization, and feedback effects on pulse stability. In dense suspensions, transient

conductivity above 0.5 kV/cm has been reported due to ion efflux and osmotic swelling, and reduced molecular uptake in multicellular clusters has been observed [10–13].

The main contribution of this study is to examine the influence of cell concentration on pulsed current during PEF applications as well as its influence on cell viability, proliferation, and metabolism; to identify the optimal cell number per cuvette; and to highlight the impact of cell concentration on electroporation.

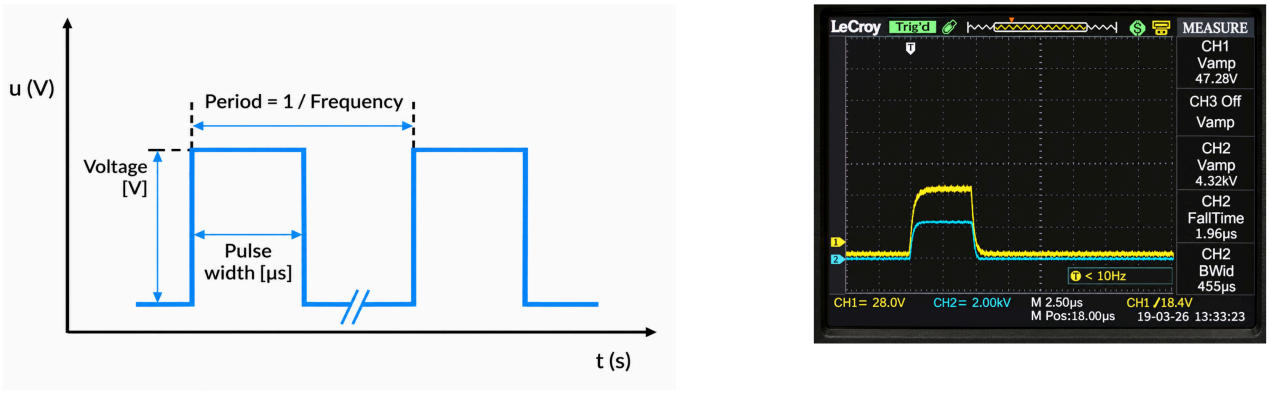
## 2. Materials and Methods

### *2.1. Cell Culture*

All procedures in which cells were exposed to air were performed in a laminar-flow cabinet (Faster BHG2006, Ferrara, Italy). An immortalized line of fibroblasts L929 (strain L, from a mouse) was cultured in T-Flasks of 25 $cm^2$ (Thermo Fisher Scientific, Waltham, MA, USA), with 5 mL of high-glucose Dulbecco's Modified Eagle Medium with L-Glutamine (DMEM, Sigma-Aldrich, Taufkirchen, Germany) containing 10% (*v*/*v*) of inactivated Fetal Bovine Serum (FBS) (Sigma Aldrich, Taufkirchen, Germany) and 1% of 10,000 U/mL Penicillin-Streptomycin (Gibco, Grand Island, NY, USA), maintained at 37 °C, 5% $CO_2$ and 95% humidity (CB150, BINDER, Tuttlingen, Germany). When cultures reached ~80% confluence under the microscope (Axiovert 40 CFL, Zeiss, Jena, Germany), cells were detached with ethylenediaminetetraacetic acid (EDTA) 25% and phenol red (Trypsin-EDTA, Gibco, Grand Island, NY, USA), centrifuged (Universal 32, Hettich, Tuttlingen, Germany), and subcultured under the same conditions until the fourth passage, when they were prepared for PEF experiments.

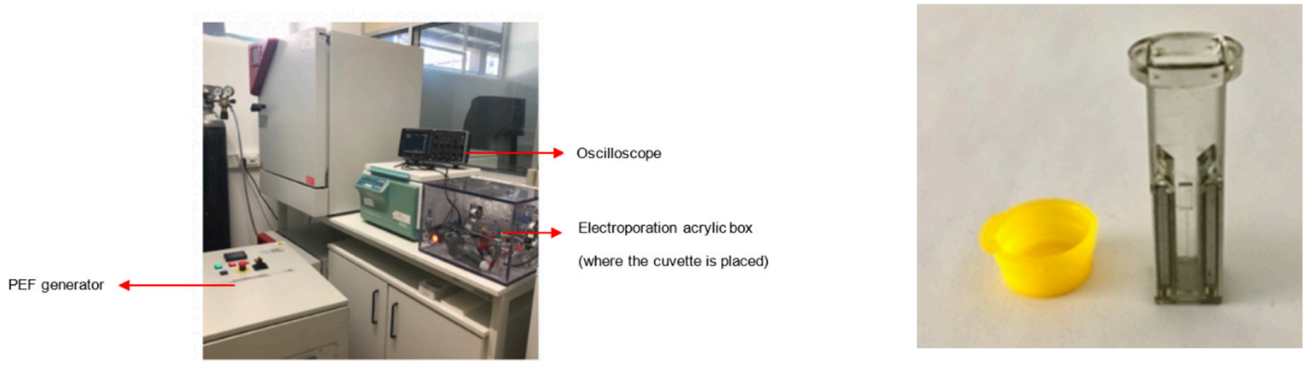
### *2.2. PEF Experiments*

All PEF experiments were conducted using a monopolar pulse generator, the EPULSUS-LPM1B-10 (Energy Pulse Systems, Lisbon, Portugal), based on a solid-state Marx generator that produces almost rectangular pulses [14] (Figure 1), and electroporation cuvettes with an 800 µL capacity and a 4 mm electrode gap (VWR, Radnor, PA, USA) (Figure 2). Cells were resuspended inside the cuvettes in 800 µL of Dulbecco's phosphate-buffered saline (DPBS, Gibco, Grand Island, NY, USA) and placed in an acrylic box where they were exposed to a PEF. Electrical parameters and peak current were set and read using the PEF equipment display and a digital oscilloscope (WaveAce, LeCroy, Chestnut Ridge, NY, USA).




(**a**) (**b**)

**Figure 1.** (**a**) Theoretical pulsed waveform. (**b**) Example 5 µs pulse current (yellow) and voltage (blue) for the applied PEF protocol, 2 kV/div, 100 A/div and 2.5 µs/div.




(**a**) (**b**)

**Figure 2.** (**a**) EPULSOS-LPM1B-10 equipment inside the culture room and (**b**) electroporation cuvette.

To study how the number of fibroblasts under PEF conditions could impact cell viability, proliferation, and metabolism, the electrical parameters were kept constant and set as follows: electric field = 10 kV/cm, number of pulses (n) = 5, pulse width ($\tau$) = 5 µs, and frequency ($f$) = 1 Hz. Five experimental groups were defined according to the number of cells, each including three replicates and both negative and positive controls. The negative control group was processed identically to the PEF groups, except that it was placed in the acrylic box without PEF exposure, while the positive control consisted of cells with severe damage and lysis, induced by three cycles of freezing (at −80 °C) and thawing (in a warm bath). Groups were as follows: $1.0 \times 10^6$, $5.0 \times 10^5$, $2.5 \times 10^5$, $1.0 \times 10^5$, and $5.0 \times 10^4$ cells.

For all PEF experiments, L929 fibroblasts at the 4th passage were used. Cells were rinsed with DPBS (Gibco, Grand Island, NY, USA) and detached enzymatically with a trypsin-EDTA solution (Gibco, Grand Island, NY, USA) for no longer than 3 min. After trypsinization, the volume was doubled with complete DMEM (Sigma-Aldrich, Taufkirchen, Germany) and then centrifuged at 1700 RPM for 9 min (Universal 32, Hettich, Tuttlingen, Germany). Cells were counted and apportioned at the desired cell number into 1.5 mL Eppendorf Safe-Lock Tubes (Eppendorf SE, Hamburg, Germany) with 800 µL of DPBS. These tubes were maintained at a low temperature of 4 °C in the refrigerator for 10 min before starting the PEF assays and were then transferred to an icebox inside the laminar-flow cabinet. After PEF treatment, cells in DPBS were kept at 4 °C on ice. Part of the suspension was used to determine cell number and viability, and the remaining cells were seeded into 24-well adherent plates (Thermo Fisher Scientific, Waltham, MA, USA) with complete medium and cultured in a $CO_2$ incubator (CB150, BINDER, Tuttlingen, Germany). Each plate was seeded with 28,500 living cells (7500 cells per $cm^2$) in wells of 3.8 $cm^2$ and monitored for 72 h.

### *2.3. Study of Electric Outputs*

The electrical analysis of PEF treatment was based on readings obtained directly from the PEF equipment display. The electrical parameters, voltage (U), pulse width ($\tau$), pulse number (n), and frequency ($f$), were kept constant across all treatment groups, except for in the negative control group (not exposed to electric fields). For each sample and condition, the energy per pulse (W), total energy ($W_t$), specific energy ($W_s$), and temperature increase ($\Delta T$) were calculated [7] using the following equations.

The electric field strength (E) was determined according to:

$$E = \frac{U}{d}, \quad (1)$$

where E, the field amplitude, is expressed in kV/cm, U is the applied pulse voltage (kV), and d is the distance between electrodes in the cuvette (cm). Electrical pulses of width τ (μs) were applied sequentially, with total treatment time calculated as:

$$t = n \cdot \tau, \tag{2}$$

with n representing the number of pulses and τ representing the pulse width (μs). Energy delivered per pulse was defined by:

$$W = U \cdot I \cdot \tau, \tag{3}$$

where W is expressed in Joules (J), U is the applied pulse voltage (kV), I is the resulting pulse current (A), and τ is the pulse width (μs). Current through the treatment medium was determined by:

$$I = \frac{U \cdot A_c \cdot \sigma}{d}, \tag{4}$$

where $A_c$ is the electrode contact area ($cm^2$), σ is the electrical conductivity (S/cm), and d is the electrode gap (cm). To account for minor variations in conductivity during treatment, average conductivity values were used throughout the calculations. Total energy delivered across all pulses was expressed as:

$$W_t = W \cdot n, \tag{5}$$

where $W_t$ is the total energy (J), and n is the number of pulses applied. Specific energy, a critical parameter for biological treatment standardization, was calculated as:

$$W_s = \frac{W_t}{V \cdot \rho}, \tag{6}$$

where $W_s$ is expressed in kJ/kg, V is the treatment chamber volume (mL), and ρ is the density of the treatment medium (kg/mL). The temperature increases in each sample, resulting from electrical energy dissipation, are given by:

$$\Delta T = \frac{W_s}{C_p}, \tag{7}$$

where $C_p$ is the specific heat capacity (kJ/(kg·°C)) of the treated material, which was taken as 4.18 kJ/(kg·°C), similar to that of water.

The relationship between average temperature and cell concentration was assessed by simple linear regression, with the coefficient of determination ($R^2$) used to quantify the strength of the association.

### 2.4. Cell Viability and Proliferation Assays

Cell viability assays were conducted using a trypan blue exclusion assay with 0.4% trypan blue (Gibco, Grand Island, NY, USA) and a hematocytometer (Hirschmann-Laborgeräte, Eberstadt, Germany) under an inverted phase-contrast microscope (Axiovert 40 CFL, Zeiss, Jena, Germany). Cell viability was assessed before PEF exposure, immediately after PEF exposure, and 72 h after PEF exposure. The total number of cells, the number of living cells, and the number of dead cells were determined according to the formula:

$$Cell\ Concentration = \frac{n\ cells \times df \times v}{hemocytometer\ field\ volume}, \tag{8}$$

where n is the number of cells counted in the hemocytometer, v (mL) represents the total volume of cell solution and pellet, and the hemocytometer field volume is defined by the manufacturer as 0.0001 mL. The dilution factor (df) was calculated using the formula below, where the initial volume equals the sample volume and the final volume equals the sum of the sample volume and the blue trypan volume (mL).

$$f = \frac{final\ volume}{initial\ volume}, \tag{9}$$

Cell viability (%) was given by the number of living cells divided by the total number of cells (live and dead).

$$Cell\ Viability = \frac{n\ living\ cells}{n\ total\ cells} \times 100, \tag{10}$$

Statistical analysis was performed using one-way analysis of variance (ANOVA), using means and standard deviation to compare sample and positive-control values with the negative control, using Microsoft Excel (Microsoft Corp., Redmond, WA, USA).

### *2.5. FTIR Spectroscopy and Multivariate Analysis*

Triplicates of Fourier-transform infrared (FTIR) spectra of both cell culture supernatant and cell pellets from each sample were collected. For each analysis, 25 µL of the sample was placed in a 96-well silicon (Si) plate and dehydrated for approximately 3 h in a vacuum desiccator (ME 2, VACUUBRAND, Wertheim, Germany). FTIR spectra were acquired using a VERTEX 70 spectrometer (Bruker, Ettlingen, Germany) equipped with an HTS-XT module (Bruker, Ettlingen, Germany). Data were acquired using OPUS 6.5 software (Bruker, Ettlingen, Germany). The resulting spectra were preprocessed using atmospheric correction, second derivatives based on the Savitsky-Golay algorithm, and unit-vector normalization. Spectral preprocessing and principal component analysis (PCA) were conducted using Unscrambler X software (software version 11.0.; Camo Analytics, Oslo, Norway). One-way analysis of variance (ANOVA) and a Student's t-test were conducted with Excel (Microsoft Corp., Redmond, WA, USA).

## 3. Results and Discussion

For the assay, cells at five different concentrations, $1.0 \times 10^6$ cells/800 µL, $5.0 \times 10^5$ cells/800 µL, $2.5 \times 10^5$ cells/800 µL, $1.0 \times 10^5$ cells/800 µL, and $5.0 \times 10^4$ cells/800 µL, were exposed to microsecond pulsed electric field stimulation (µsPEF), using constant electrical parameters: electric field = 10 kV/cm, number of pulses (n) = 5, pulse width ($\tau$) = 5 µs and frequency ($f$) = 1 Hz. These settings correspond to an intermediate energy regime for mammalian cells, minimizing the risk of Joule heating or short-circuiting. A high electric field (E), combined with short pulse widths and low frequency, confines energy delivery to non-thermal bioeffects and limits thermal dissipation [15–17].

Mouse fibroblast L929 cells were used as a model because of their high reproducibility and experimental consistency. Unlike primary fibroblasts, which exhibit donor variability and limited expansion, L929 cells provide consistent membrane electroporation responses and metabolic stability under PEF conditions [16,18]. Dulbecco's phosphate-buffered saline (DPBS; Gibco, Grand Island, NY, USA) was used as the conductive medium inside the electroporation cuvette due to its isotonic osmolarity and pH buffering capacity, enabling uniform electric field delivery while preserving mammalian cell viability. In contrast, water is hypotonic, leading to cell lysis, and its low conductivity can cause excessive voltage drops across the sample [19]. The culture medium was excluded because its conductivity is significantly higher than that of PBS or water, thereby promoting Joule heating, bubble

formation, and electrolysis [20]. During PEF assays, cells were maintained at 4 °C. Cooling before and after PEF preserves membrane integrity, minimizes heat-induced damage from pulses, and improves measurement of immediate permeabilization before recovery processes are initiated. Returning the cuvettes to ice for 10 min after pulsing reduces temperature-sensitive stress in mammalian cells, thereby improving viability and helping to distinguish reversible from irreversible damage. Ice incubation has been reported not to delay membrane recovery or promote lysis, supporting this protocol [21,22]. Ice incubation also reduces cellular enzymatic activity, thereby arresting ongoing metabolic fluxes and preventing artifacts in subsequent FTIR spectroscopy analysis. Maintaining cells at 4 °C reduces temperature-sensitive membrane repair and leakage, thus ensuring that FTIR spectral features are indicative of acute permeabilization rather than recovery [23,24]. All assays were performed in triplicate, including negative controls (i.e., live cells were subjected to the same protocol except for PEF) and positive controls (i.e., cells were lysed by three successive cycles of freezing and thawing).

The molecular fingerprints of cells and cell culture media were obtained by FTIR spectroscopy, as this technique, particularly in the mid-infrared region, reflects the fundamental vibrational modes of a wide range of functional groups in biomolecules, including nucleic acids, proteins, carbohydrates, and lipids. This technique has high sensitivity and specificity for acquiring the sample's molecular fingerprint and has been extensively used in biomedical applications, including for discriminating cell metabolic state [25], medical diagnosis from serum samples [26], and elucidating cell death mechanisms [27]. In the present study, FTIR was used as a fingerprinting approach to compare spectral differences among treatment conditions.

### *3.1. Variations in Electrical Current and Temperature Increases at Different Cell Concentrations*

To analyze how the cell number affects current flow between the electrodes, current (A) and temperature (°C) were recorded at each of five consecutive pulses. Temperature increases were determined for every sample. For all PEF-exposed groups, the applied current varied from pulse to pulse and consistently peaked at pulse 5. In cuvettes containing $1.0 \times 10^6$ cells, the mean current intensity was 269 A, with a maximum temperature of 8.0 °C at pulse 5 and an average temperature rise of 4.47 °C. Although the conductivity and specific energy ($W_s$) could not be measured experimentally at the time of testing, they were estimated using Equations (4) and (6). Under the tested conditions, cell concentration modulated the electrical response of the suspension and was associated with the observed differences in temperature increases during PEF exposure (Table 1).

**Table 1.** Effect of cell concentration during PEF, concerning the achieved current intensity, estimated conductivity, maximum temperature, and average temperature deviation in relation to cells maintained on ice (at 4 °C).

| Number of Cells (per 0.8 mL of PBS) | I (A) | Conductivity (mS/cm) | $W_s$ (kJ/kg) | T Maximum at Pulse 5 (°C) | Average ΔT (°C) |
|---|---|---|---|---|---|
| $1.0 \times 10^6$ | 269 | 13.45 | 33.6 | 8.0 | 4.47 |
| $5.0 \times 10^5$ | 286 | 14.30 | 35.0 | 8.4 | 4.67 |
| $2.5 \times 10^5$ | 293 | 14.65 | 36.6 | 8.8 | 4.80 |
| $1.0 \times 10^5$ | 293 | 14.65 | 36.6 | 8.8 | 4.80 |
| $5.0 \times 10^4$ | 429 | 21.45 | 53.6 | 12.8 | 4.97 |

A linear fit of the average temperature increase as a function of cell concentration ($\Delta T_{avg} = -5 \times 10^{-7} \times$ [cells/mL] + 4.915; $R^2 = 0.922$) confirmed an inverse relationship. The negative slope indicates that higher cell concentrations reduce heating, and the Pearson correlation shows that approximately 92% of the variance in temperature rise is explained by the number of cells (Figure 3). In the electroporation cuvette, under the tested conditions, the results indicate a correlation among cell concentration, current-amplitude fluctuations, and temperature rise. At a constant voltage, higher cell concentrations resulted in a lower current intensity and reduced Joule heating. The observed temperature elevations were minimal and, together with maintaining samples at 4 °C, were unlikely to compromise cell viability. Even at room temperature, the estimated maximum temperatures remain well below thresholds for protein denaturation or membrane destabilization [10].

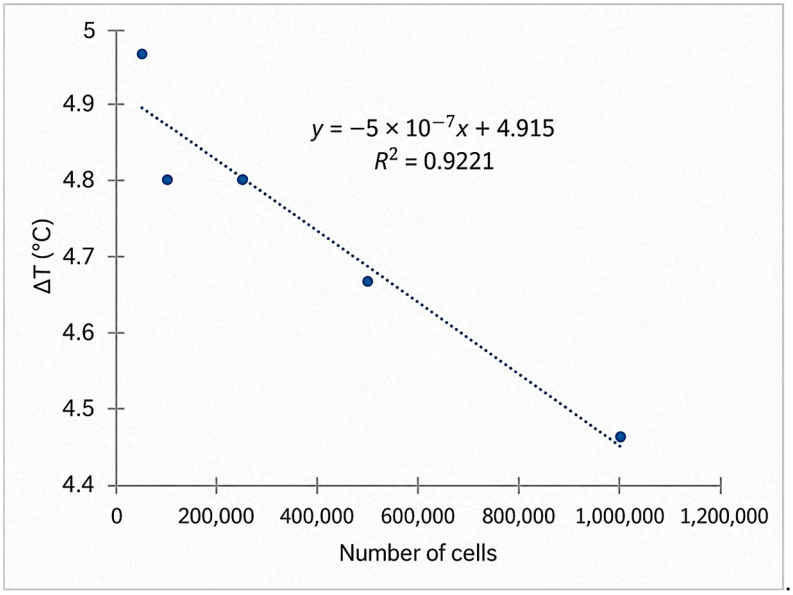



**Figure 3.** Relationship between temperature variation and cell concentration in the electroporation cuvette.

Immediate post-PEF viability patterns indicate cell-concentration-dependent susceptibility to electroporation-induced membrane permeabilization, consistent with reports that progressive increases in current and temperature are driven by transient increases in conductivity resulting from pore formation in the membrane [10]. Considering that the peak current difference between the lowest and highest cell concentration tested (429 A at $5.0 \times 10^4$ cells vs. 269 A at $1.0 \times 10^6$ cells) is approximately 37% (Table 1) and should be expected to be 1–2% (on the order of 0.2–0.6%, assuming typical fibroblast L929 cell dimensions in suspension), the magnitude of the current reduction cannot be explained by cell volume fraction alone. It can be reported that the relation between current and concentration is an observation without an established mechanism, such as localized shielding, altered specific energy absorption, and other processes, which remain plausible, but more studies are needed with direct conductivity measurements across the tested concentration range [28–30]. Overall, these results indicate that, under the tested conditions, cellular responses track cell concentration and are associated with membrane permeabilization rather than with thermal stress, which was minimal across all groups.

### 3.2. Cell Viability and Proliferation

Trypan blue exclusion analysis provided direct quantification of cell viability immediately following PEF exposure and after 72 h of recovery in culture. Negative controls, in which cells were subjected to all handling steps except the PEF, exhibited excellent baseline viability (96.3%, n = 3), whereas positive controls, exposed to three cycles of freeze-thaw, showed near-complete lysis (65–92% lysed) as expected. High-concentration groups of $1.0 \times 10^6$ and $5.0 \times 10^5$ cells maintained >79% recovery and >85% viability immediately post-PEF; in contrast, lower concentrations showed progressive declines (Table 2). Cell lysis and membrane disruption induced by PEF were <8% in groups of $1.0 \times 10^6$ cells, while groups of $1.0 \times 10^5$ and $5.0 \times 10^4$ exhibited higher cell lysis (40% and 65%), comparable to the positive control samples for each group.

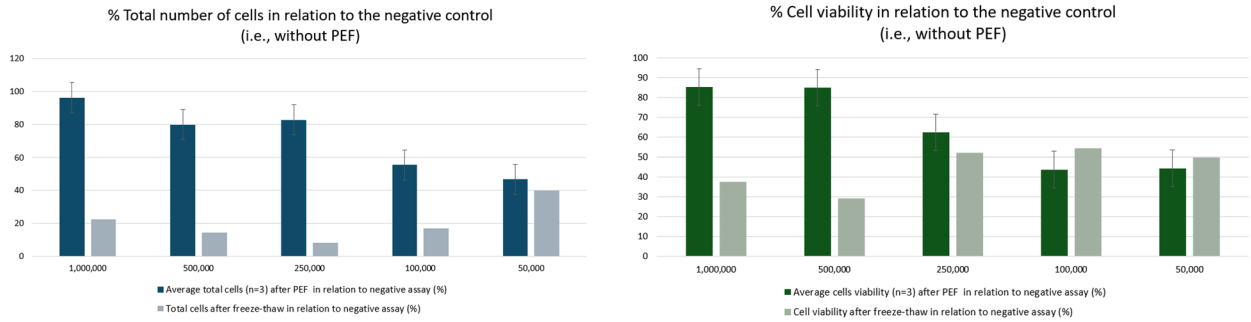
**Table 2.** Statistical data (percentage) for number of cells and viability, with average (AV) and standard deviation (SD) for each group and for the positive control (freeze-thaw) in relation to the negative control (i.e., conducted without a PEF).

| Cells Used in the Assay | Average Cells (n = 3) After PEF | Standard Deviation (n = 3) of Cells After PEF | Cells After Freeze-Thaw | Average Cell Viability (n = 3) After PEF | Standard Deviation of Cell Viability (n = 3) After PEF | Cell Viability After Freeze-Thaw |
|---|---|---|---|---|---|---|
| Results immediately after the PEF assay in relation to the assay without PEF (%) | | | | | | |
| $1.0 \times 10^6$ | 97 | 11 | 22 | 85 | 3 | 38 |
| $5.0 \times 10^5$ | 80 | 2 | 14 | 85 | 11 | 29 |
| $2.5 \times 10^5$ | 83 | 13 | 8 | 63 | 5 | 52 |
| $1.0 \times 10^5$ | 56 | 10 | 17 | 44 | 27 | 55 |
| $5.0 \times 10^4$ | 47 | 12 | 40 | 44 | 10 | 50 |
| Results after 72 h of cell culture following PEF in relation to the assay without PEF (%) | | | | | | |
| $1.0 \times 10^6$ | 80 | 10 | 70 | 98 | 8 | 79 |
| $5.0 \times 10^5$ | 91 | 11 | 26 | 87 | 7 | 80 |
| $2.5 \times 10^5$ | 88 | 7 | 8 | 86 | 5 | 71 |
| $1.0 \times 10^5$ | 92 | 4 | 3 | 78 | 5 | 0 |
| $5.0 \times 10^4$ | 54 | 4 | 5 | 74 | 13 | 51 |

Immediately following PEF treatment, cultures seeded at $1.0 \times 10^6$ cells demonstrated an average total cell recovery of 96.30% ± 11.11% relative to non-treated controls, with post-PEF viability averaging 85.35% ± 3.45% (mean ± SD, n = 3). At $5.0 \times 10^5$ cells, comparable total cell recovery (79.76% ± 2.06%) and viability (85.16% ± 11.07%) were observed. The $2.5 \times 10^5$ group exhibited a slightly lower immediate recovery (82.67% ± 12.86% of total cells) and a viability of 62.54% ± 5.34%. At $1.0 \times 10^5$ cells, total cell recovery averaged 55.56% ± 9.62% with post-PEF viability of 43.94% ± 27.40%, suggesting increased susceptibility to PEFs at lower initial concentrations. The lowest-concentration condition ($5.0 \times 10^4$ cells/800 µL) showed the most pronounced immediate impact, with a total cell recovery of 46.67% ± 11.55% and a viability of 44.44% ± 9.62%.

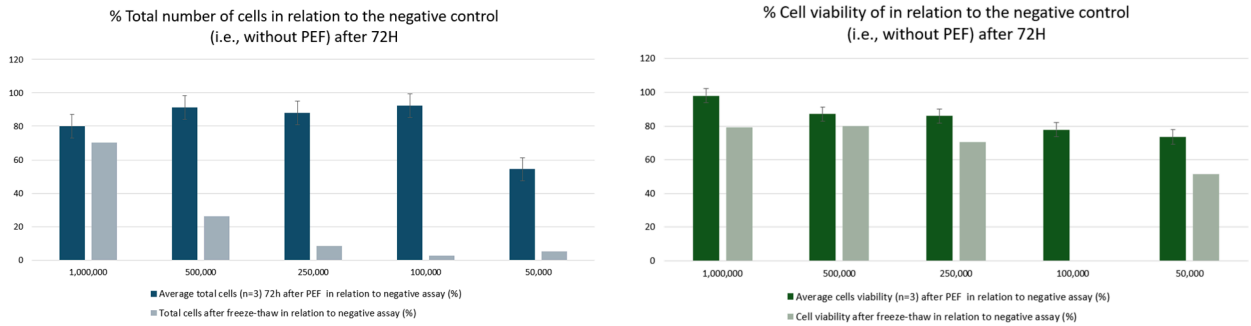
A small fraction of cells from the positive control survived (Figure 4), even after three freeze-thaw cycles. Higher cell concentrations are more resistant to freeze-thaw-induced damage, including intracellular ice formation and dehydration without bursting, partly due to cytoskeletal modulation and endogenous stabilizers such as trehalose (an osmoprotectant and metabolic regulator) [31]. Survival in the positive (freeze-thaw) control was not uniform across groups, ranging from approximately 0% to 80% at 72 h (Figure 5). This control is therefore better regarded as a severe, variable-damage benchmark than as an absolute

standard for complete lysis, and comparisons that assume uniform freeze-thaw damage across groups should be interpreted with this variability in mind. Even though no genetic study was conducted, it can be argued whether the surviving population could exhibit genomic instability, with karyotype changes that can influence cell proliferation [32]. Endogenous stabilizers such as trehalose [31] may contribute to the partial survival observed, but confirming this would require dedicated genomic or karyotyping assays.




(**a**) (**b**)

**Figure 4.** (**a**) Average number of cells and (**b**) viability of assays conducted immediately after the assay with different groups in relation to the negative control (assay without a PEF). The error bars are the average value of the standard deviation (SD) of all assays.




(**a**) (**b**)

**Figure 5.** (**a**) Average number of cells and (**b**) viability of assays conducted 72 h after PEF assay with different groups in relation to the negative control (assay without a PEF). The error bars are the average value of the standard deviation (SD) of all assays.

To assess longer-term viability and proliferation, cells were monitored at 72 h. Monitoring fibroblasts at 72 h post-PEF enables discrimination between enhanced growth (reversible electroporation) and persistent death (irreversible electroporation), which can be difficult to detect at 24 h or 48 h endpoints [16,28]. After 72 h in culture, recovery cultures demonstrated substantial phenotypic resilience in all replicates (Figure 4). At $1.0 \times 10^6$ cells, 72 h post-PEF, total cells reached 80.00% ± 10.00% of control values, with a recovered viability of 98.00% ± 7.61%. At $5.0 \times 10^5$ cells, equivalent recovery patterns were observed (total cells = 91.22% ± 10.96% of control, with viability = 87.06% ± 7.37%). The $2.5 \times 10^5$ group recovered to 87.96% ± 6.99% total cells with 86.03% ± 4.60% viability. Even under the $1.0 \times 10^5$ cells/800 µL condition, which showed the lowest immediate viability, cells recovered substantially after 72 h (92.31% ± 4.44% total cells, 77.89% ± 4.63% viability). The $5.0 \times 10^4$ group exhibited similar recovery (73.51% ± 12.90% total cells with 73.51% ± 12.90% viability) at 72 h. The time-dependent recovery observed across all conditions supports the premise that PEF-mediated membrane disruption predominantly induces transient pore formation rather than irreversible cell injury [28,33]. Overall, restoration of viability within 72 h approached or exceeded 85% across all PEF-treated

samples, indicating efficient cellular homeostatic mechanisms and active membrane repair processes, even under the lowest-concentration conditions. Such a recovery trajectory reflects sublethal stress induced by the PEF under the applied conditions, mediated by adaptive responses that map to pore resealing and metabolic restoration [34].

### *3.3. FTIR Spectroscopic Analysis*

FTIR spectroscopic analysis was conducted in triplicate for each sample at two time points: immediately after PEF application (DPBS or cell supernatant) and after 72 h (cell culture medium).

Supernatant at t = 0 h and culture media at t = 72 h from the extreme groups ($1.0 \times 10^6$ and $5.0 \times 10^5$ cells) exhibited more pronounced differences in absorbance values, with the group containing $1.0 \times 10^6$ cells showing higher absorbance. PEF-treated cells and positive controls displayed broadly similar spectral profiles.

Spectral analysis of the supernatant immediately after PEF assays showed characteristic absorption bands at wavenumbers for cellular macromolecules: amide I (1650–1680 $cm^{-1}$) and amide II (1520–1570 $cm^{-1}$) bands mostly due to proteins; C-H stretching (2850–2960 $cm^{-1}$) for the lipid and protein aliphatic chains; and phosphodiester stretches (1000–1300 $cm^{-1}$) present, e.g., in nucleic acid. Immediate post-PEF spectra from high-density cultures ($1.0 \times 10^6$ and $5.0 \times 10^5$ cells) indicated preserved amide band integrity and an unchanged lipid-to-protein ratio relative to untreated controls, indicating limited structural disruption of cell membranes and organellar components (Figures 6 and 7). Spectra from $1.0 \times 10^5$ and $5.0 \times 10^4$ cells exhibited a slight increase in the amide I band and relative intensity shifts in the phosphodiester region, indicative of localized membrane destabilization and possible protein denaturation. The comparative spectra of the cell culture medium at 72 h after PEF showed a significant recovery of cellular integrity. Protein bands were restored to baseline, as indicated by phosphodiester band positions, suggesting cell integrity [35,36].

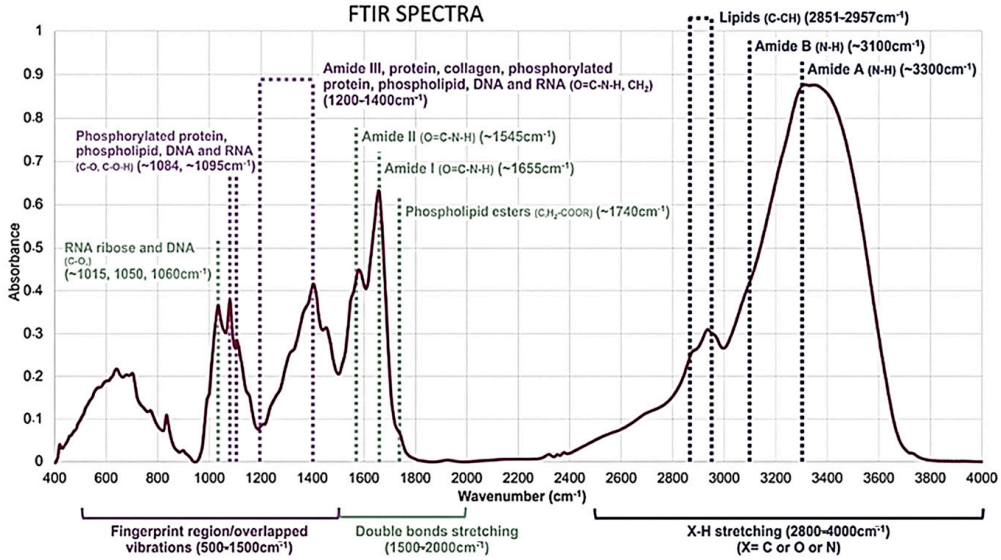



**Figure 6.** FTIR spectra with highlighted regions corresponding to specific molecular vibrations.

One-way analysis of variance (ANOVA) was performed on the absorbance spectra of the supernatant and pellet immediately after PEF application and on the culture medium after 72 h. Lower *p*-values were obtained for the NO PEF vs. PEF and NO PEF vs. freeze-thaw comparisons, whereas *p*-values were higher for PEF vs. freeze-thaw, indicating that no significant difference was detected between PEF and freeze-thaw absorbance values,

though this comparison should be read in light of the freeze-thaw control's variability (Table 3). When supernatant, pellet, and culture medium were analyzed separately after 72 h, *p*-values varied among conditions. Overall, the most promising groups for spectral discrimination were $5.0 \times 10^5$ and $1.0 \times 10^6$, and the most informative condition was the supernatant. In the $5.0 \times 10^5$ cells group, supernatant spectra were statistically different across all comparisons ($p = 0.005$, 0.0003, and 0.002), and standard deviations (SD) were low relative to the means (AV) (NO PEF: 66 ± 4, PEF: 82 ± 7, freeze-thaw: 109 ± 9), indicating a separation that is both statistically and practically meaningful. In the group of $1.0 \times 10^6$ cells, PEF values exceeded those of NO PEF but were almost indistinguishable from freeze-thaw, suggesting that the PEF does not generate a clearly distinct supernatant fingerprint. Because survival in the freeze-thaw control itself varied across groups, this comparison indicates overlap with a variable, severe-damage benchmark rather than equivalence to a fixed reference.

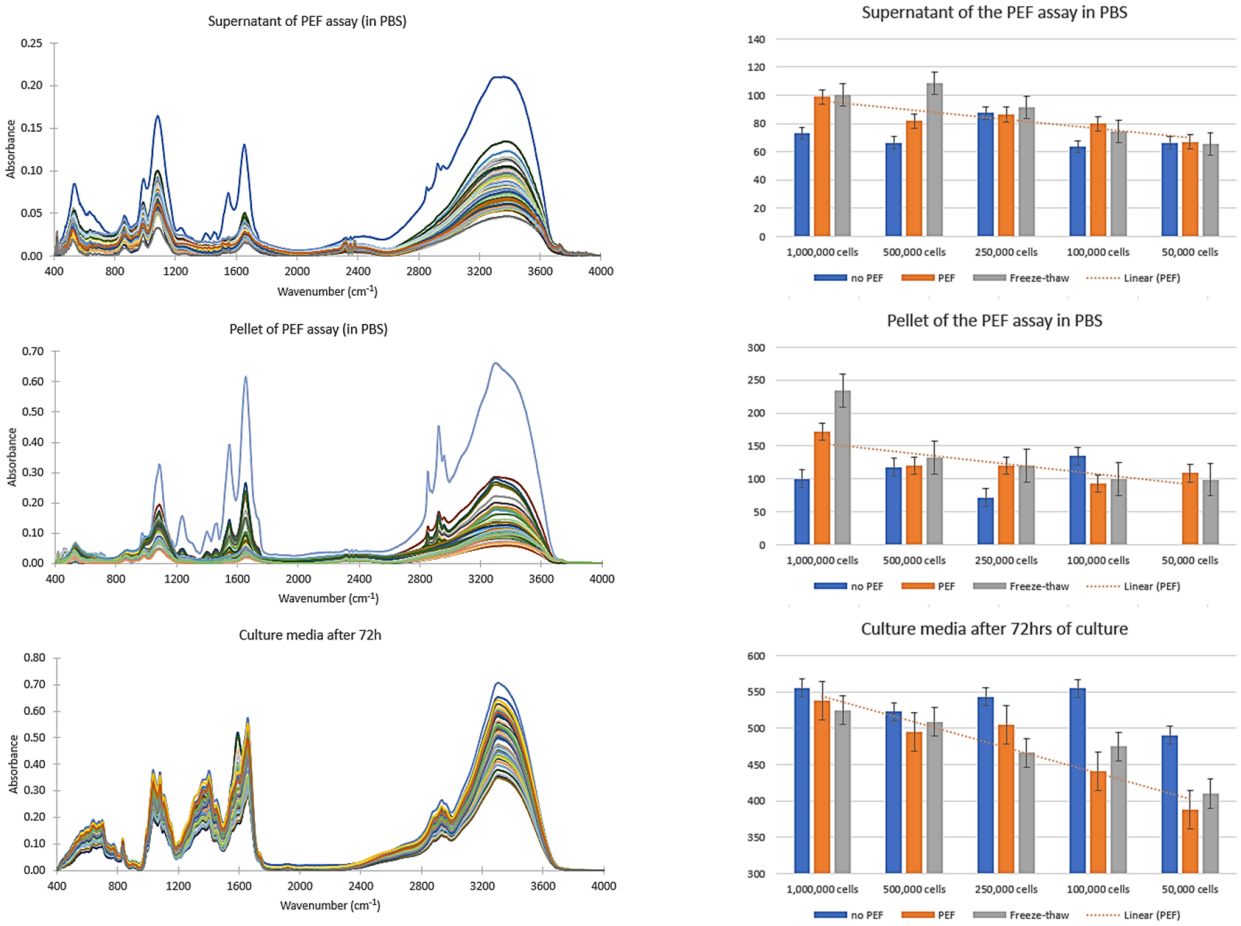



**Figure 7.** (**a**) FTIR spectra of individual replicates of the supernatant and cell pellet after PEF treatment, and of the culture medium after cell plating and 72 h of incubation following the PEF experiment. (**b**) Average sum of absorbances over the whole FTIR spectra of triplicate PEF assays for the supernatant and cell pellet immediately after PEF treatment, and FTIR spectra of the culture medium after cell plating and 72 h of incubation following the PEF experiment.

Principal component analysis (PCA) was performed on normalized second-derivative spectra of the supernatant and cell pellet immediately after PEF application and on culture media after 72 h. Sample clusters were examined as a function of treatment (NO PEF, PEF, freeze-thaw) and cell number and emphasize biochemical composition rather than

metabolite concentration or apoptotic body abundance. The results suggest that cell metabolism was influenced by the cell concentration used during PEF application. The two PCA score plots (Figure 8) summarize the variance in normalized second-derivative spectra of the supernatant (DPBS) collected immediately after treatment. Second-derivative preprocessing is widely used in spectroscopy to reduce baseline effects and enhance subtle, overlapping spectral features, making separations more consistent with differences in spectral shape and fine structure than with simple intensity scaling [37]. PCA plots show that most of the variance (64%) is captured, and the structure is clear: untreated samples cluster mainly on negative PC1, PEF-treated samples cluster mainly on positive PC1, and freeze-thawed samples lie closer to the center with partial overlap. This pattern supports the interpretation that the PEF condition is the dominant source of variation in the supernatant fingerprint. This is consistent with the idea that electroporation can alter membrane permeability and promote the release of intracellular constituents, shifting extracellular composition [36]. The Hotelling ellipse indicates that the main cluster separation is not driven solely by a single extreme point, although a small number of observations appear near or beyond the boundary corresponding to outliers. In the cell number PCA panel, most groups overlap, except for samples with $1.0 \times 10^6$, suggesting that cell number contributes less to variance than treatment and that any cell number effect is weaker, nonlinear, or distributed across higher components [38].

**Table 3.** Average (AV) and standard deviation (SD) of absorbances of the sum of whole FTIR spectra of PEF assays concerning the supernatant and the cell pellet of the assay immediately after PEF application and from culture media grown for 72 h.

| Sample | Number of Cells Used in PEF Assay | Without PEF | | With PEF | | Freeze-Thaw | | *p*-Value of ANOVA (if <0.1) | | |
|---|---|---|---|---|---|---|---|---|---|---|
| | | AV | SD | AV | SD | AV | SD | PEF vs. NO PEF | PEF vs. Freeze-Thaw | NO PEF vs. Freeze-Thaw |
| Supernatant | $1.0 \times 10^6$ | 73 | 15 | 99 | 17 | 100 | 24 | 0.044 | ns | ns |
| | $5.0 \times 10^5$ | 66 | 4 | 82 | 7 | 109 | 9 | 0.005 | 0.0003 | 0.002 |
| | $2.5 \times 10^5$ | 87 | 8 | 86 | 21 | 91 | 7 | ns | ns | ns |
| | $1.0 \times 10^5$ | 64 | 3 | 80 | 13 | 74 | 12 | 0.058 | ns | ns |
| | $5.0 \times 10^4$ | 66 | 19 | 67 | 9 | 65 | 10 | ns | ns | ns |
| Pellet | $1.0 \times 10^6$ | 100 | 19 | 172 | 46 | 234 | 7 | 0.019 | 0.049 | 0.0003 |
| | $5.0 \times 10^5$ | 118 | 41 | 120 | 13 | 132 | 6 | ns | ns | ns |
| | $2.5 \times 10^5$ | 71 | 2 | 120 | 29 | 119 | 13 | 0.019 | ns | 0.0032 |
| | $1.0 \times 10^5$ | 134 | 25 | 93 | 8 | 100 | 8 | 0.0023 | ns | 0.082 |
| | $5.0 \times 10^4$ | * | * | 109 | 29 | 99 | 5 | ns | ns | ns |
| Culture media after 72 h | $1.0 \times 10^6$ | 555 | 86 | 538 | 57 | 525 | 44 | ns | ns | ns |
| | $5.0 \times 10^5$ | 523 | 28 | 494 | 35 | 509 | 12 | ns | ns | ns |
| | $2.5 \times 10^5$ | 543 | 35 | 505 | 19 | 466 | 53 | 0.033 | 0.075 | 0.10 |
| | $1.0 \times 10^5$ | 555 | 56 | 441 | 28 | 474 | 48 | 0.0077 | ns | ns |
| | $5.0 \times 10^4$ | 490 | 57 | 388 | 42 | 410 | 31 | 0.0069 | ns | 0.099 |

* FTIR spectra considered outliers and not considered. ns: not significant

PCA score plots of the normalized second-derivative spectra of the pellet measured immediately after treatment (Figure 9) show that PC1 accounts for 65% of the variance and PC2 for 17%, indicating that most of the spectral structure is captured in the two-dimensional score space. In the treatment plot, untreated pellets cluster primarily in the upper-right quadrant, whereas freeze-thaw samples are shifted left (more negative PC1) and tend to cluster around slightly negative PC2. The PEF group covers a much larger region, spanning both sides of PC1 and extending further into the negative PC2 than the other conditions do. This suggests that PEF treatment influences the pellet fingerprint, producing greater heterogeneity in pellet spectra than samples from the negative control group (i.e., without PEF) and the positive control group (i.e., freeze-thawing). This heterogeneity is consistent with a range of cellular outcomes after PEF exposure, ranging from limited

permeabilization to more extensive structural disruption, which would plausibly alter the chemical and physical composition retained in the pellet. In the cell number plot, the groups overlap substantially, so cell numbers do not generate discrete clusters. However, the highest cell numbers occur more frequently in the lower-right quadrant (positive PC1, negative PC2), whereas lower cell numbers occur more frequently in the left and upper quadrants, suggesting that cell number contributes partially to the variance explained by PC1 and PC2. A Hotelling ellipse at 5% is overlaid, providing a visual boundary for unusually positioned observations without, by itself, implying causality [36–38].

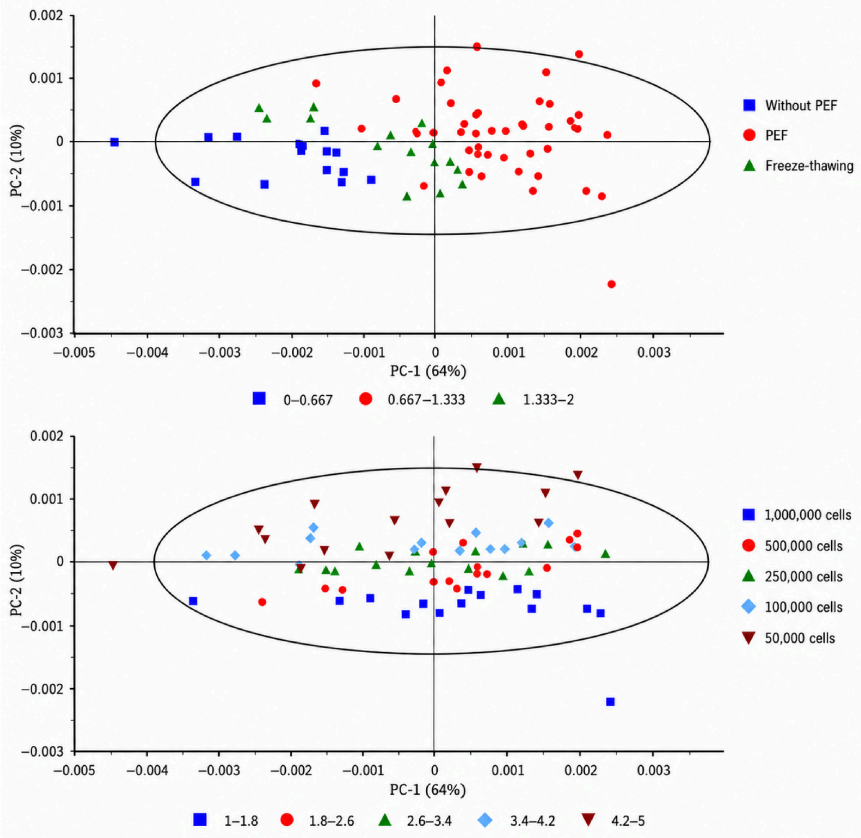



**Figure 8.** PCA of normalized second-derivative spectra of supernatant immediately after PEF. The Hotelling ellipse at 5% is represented.

PCA of normalized second-derivative spectra of culture media sampled 72 h after treatment (Figure 10) shows that PC1 accounts for 75% of the variance and PC2 for 9%, indicating that the dominant separation is along PC1. PC2 captures smaller differences among all groups rather than the main effect. Second-derivative preprocessing reduces baseline effects and highlights subtle spectral characteristics, indicating that score differences are more consistent with changes in spectral shape than with simple intensity offsets. In the PEF treatment scores, freeze-thaw samples are displaced toward positive PC1 and exhibit the widest spread, whereas several freeze-thaw observations are near or outside the Hotelling ellipse and were therefore treated as outliers. By contrast, PEF-treated and untreated samples overlap strongly and cluster around slightly negative PC1. The 72 h media fingerprint of the PEF appears comparatively modest, converging with the untreated profile over 72 h. In the cell number panel, all concentrations overlap; however, the highest PC1 scores occur primarily at the highest seeding levels, with intermediate concentrations closer to the origin. This pattern suggests that cell concentration contributes to the dominant variance direction in culture media and modulates the most extreme PC1 values, without generating discrete clusters on its own [37,38].

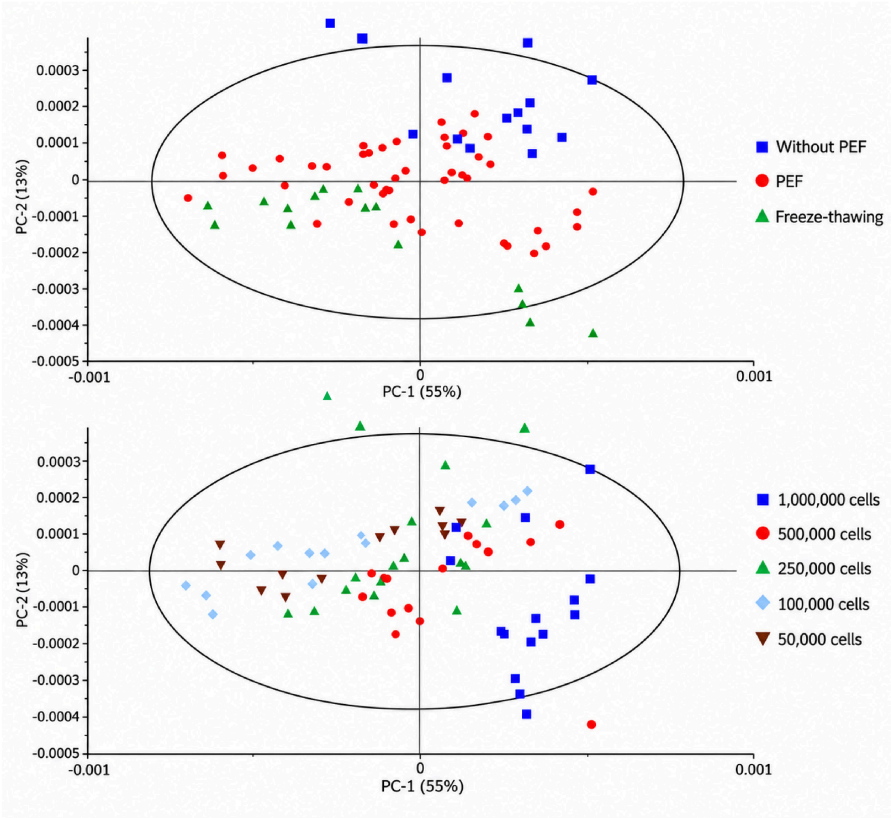



**Figure 9.** PCA of normalized second-derivative spectra of the pellet immediately after PEF. The Hotelling ellipse at 5% is represented.

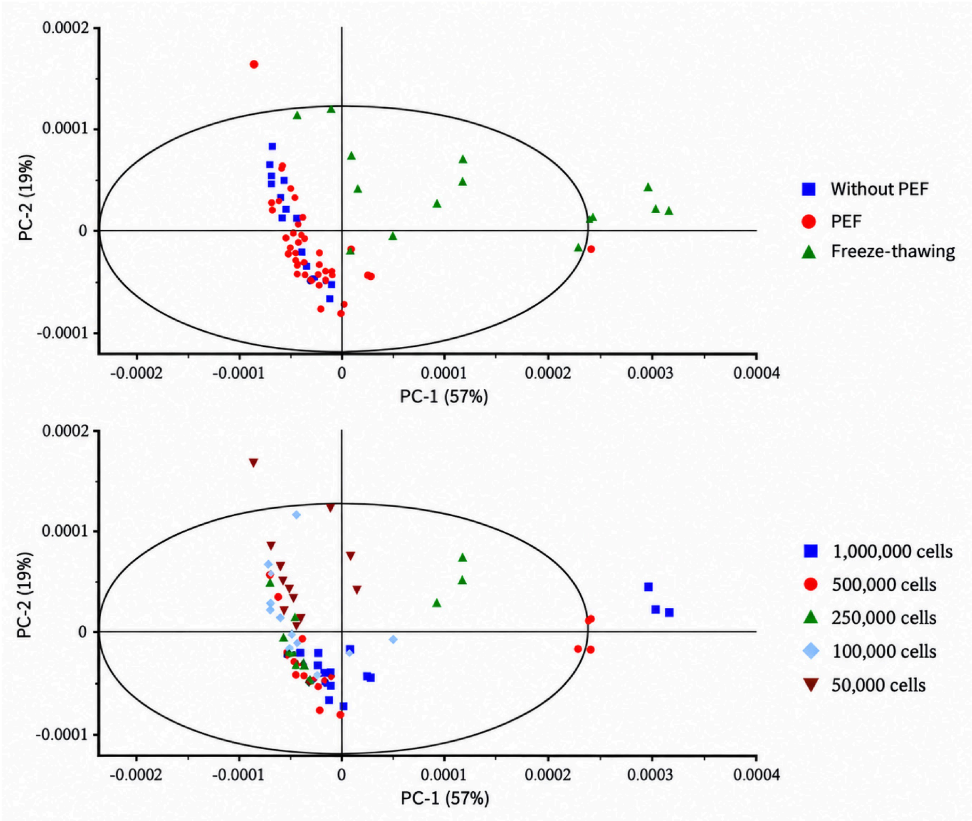



**Figure 10.** PCA of normalized second-derivative spectra of culture media 72 h after PEF application. The Hotelling ellipse at 5% is represented.

## 4. Conclusions

The main goal of the present work was to investigate the effect of cell concentration on the electrical response, immediate viability, post-treatment recovery, and FTIR spectral profiles of L929 mouse fibroblasts exposed to a fixed microsecond pulsed electric field (μsPEF) protocol. Five cell concentrations, ranging from $5.0 \times 10^4$ to $1.0 \times 10^6$ cells in 800 μL of DPBS, were evaluated under the same nominal electrical conditions: 10 kV/cm, five pulses, 5 μs pulse width, and 1 Hz frequency.

Under the experimental conditions investigated, cell concentration was associated with relevant differences in the measured electrical and biological responses. Higher cell concentrations were associated with lower peak current, smaller temperature increases, and higher immediate post-PEF viability. For example, the mean peak current decreased from 429 A at $5.0 \times 10^4$ cells to 269 A at $1.0 \times 10^6$ cells, while the corresponding maximum temperature rise decreased from 12.8 °C to 8.0 °C. The linear association observed between cell concentration and average temperature increase should, however, be interpreted as a limited relationship under the conditions tested and not as evidence of a fully established causal mechanism. In particular, conductivity was estimated rather than directly measured for each condition.

Immediate post-PEF viability also varied with cell concentration. The highest-concentration groups showed the highest viability, whereas the lowest-concentration groups showed the greatest immediate loss of viability. After 72 h of recovery culture, all PEF-treated groups retained viable cells and showed substantial recovery relative to their immediate post-treatment status, with viability values ranging from approximately 73.5% to 98.0%. These findings are consistent with a substantial reversible or sublethal component of the response under the tested conditions. Nevertheless, because no permeabilization-specific assay was performed, the present data do not establish membrane resealing or reversible electroporation as a definitive mechanism. The results should therefore be described as compatible with, rather than conclusive proof of, predominantly reversible membrane perturbation.

FTIR spectroscopy and PCA showed that macromolecular release was transient and that the biochemical profile trended toward that of the negative control after PEF, distinguishing these effects from the irreversible damage caused by freeze-thaw cycles. The freeze-thaw condition provided a severe-damage reference, but its variable residual survival indicates that it should not be regarded as an absolute standard for complete lysis. Comparisons between PEF and freeze-thaw samples should therefore be interpreted as comparisons with a variable damage benchmark rather than as evidence that the two treatments produce equivalent biological effects.

These findings should be interpreted within the scope of the experimental conditions investigated, namely a single cell line (L929), a single PEF protocol (10 kV/cm (5 pulses, 5 μs, 1 Hz)), a single cuvette geometry, and a single suspension buffer (DPBS). Confirmation in other cell models, PEF protocols, and clinically relevant experimental conditions is required.

Overall, the findings indicate that cell concentration is an important experimental and process parameter when designing and interpreting μsPEF protocols for suspended mammalian cells. In the tested L929-DPBS model and under the specific pulse conditions used, higher cell concentrations were associated with lower measured electrical and thermal responses and improved immediate cell viability, while all tested concentrations showed measurable recovery during the 72 h observation period. These observations may inform the design of future biomedical engineering and tissue-engineering studies, but they do not, by themselves, establish an optimal cell concentration for clinical translation or for other electroporation applications. The conclusions are limited to the experimental system investigated, one immortalized cell line, one suspension medium, one cuvette

geometry, and one nominal PEF protocol, and the measurement methods used. Further studies should include direct, condition-specific conductivity measurements; a validated permeabilization assay; a rigorously characterized positive-control condition; additional time points; and confirmation in other cell models and application-relevant systems. These studies will be necessary to determine the mechanisms underlying the concentration-dependent electrical response and to assess the generalizability and translational relevance of the present observations.

**Author Contributions:** Conceptualization, V.M.C., C.R.C.C. and L.M.S.R.; methodology, V.M.C., C.R.C.C. and L.M.S.R.; investigation, V.M.C.; formal analysis, V.M.C. and C.R.C.C.; writing—original draft preparation, V.M.C.; writing—review and editing, C.R.C.C. and L.M.S.R. All authors have read and agreed to the published version of the manuscript.

**Funding:** This research was partially supported by Instituto Politécnico de Lisboa, IDI&CA/IPL/2017/DrugsPlatf/ISEL, 2018/RenalProg/ISEL, and 2020/NephroMD, in close cooperation with Energy Pulse Systems. Experiments were conducted at the Research & Development Laboratory in Health and Engineering, ISEL, using PEF equipment provided by Energy Pulse Systems.

**Institutional Review Board Statement:** Not applicable.

**Informed Consent Statement:** Not applicable.

**Data Availability Statement:** Data are contained within the article.

**Acknowledgments:** AI tools were used for language editing and improving clarity. The scientific content and results are entirely the author's own work.

**Conflicts of Interest:** Author Luis Redondo is affiliated with the company EnergyPulse Systems (EPS). The remaining authors declare no conflicts of interest.

## References

1. Kotnik, T.; Kramar, P.; Pucihar, G.; Miklavčič, D.; Tarek, M. Cell membrane electroporation—Part 1: The phenomenon. *IEEE Electr. Insul. Mag.* **2012**, *28*, 14–23. [CrossRef]
2. Feng, Y.; Yang, T.; Zhang, Y.; Zhang, A.; Gai, L.; Niu, D. Potential applications of pulsed electric field in the fermented wine industry. *Front. Nutr.* **2022**, *9*, 1048632. [CrossRef] [PubMed]
3. Qu, S.; Ke, Q.; Li, X.; Yu, L.; Huang, S. Influences of pulsed electric field parameters on cell electroporation and electrofusion events: Comprehensive understanding by experiments and molecular dynamics simulations. *PLoS ONE* **2025**, *20*, e0306945. [CrossRef] [PubMed]
4. Laustsen, A.; Bak, R.O. Electroporation-based CRISPR/Cas9 gene editing using Cas9 protein and chemically modified sgRNAs. In *CRISPR Gene Editing: Methods and Protocols*; Luo, Y., Ed.; Methods in Molecular Biology; Humana Press: New York, NY, USA, 2019; Volume 1961. [CrossRef] [PubMed]
5. Aycock, K.N.; Davalos, R.V. Irreversible electroporation: Background, theory, and review of applications. *J. Med. Devices* **2019**, *13*, 020801. [CrossRef]
6. Hadzialjevic, B.; Omerzel, M.; Trotovsek, B.; Cemazar, M.; Jesenko, T.; Sersa, G.; Djokic, M. Electrochemotherapy combined with immunotherapy: A promising potential in the treatment of cancer. *Front. Immunol.* **2024**, *14*, 1336866. [CrossRef] [PubMed]
7. Salvador, D.; Almeida, H.; Rego, D.; Mendonça, P.; Sousa, A.P.; Serra, M.; Redondo, L. Pulsed electric fields for valorization of platelets with no therapeutic value towards a high biomedical potential product: A proof of concept. *Appl. Sci.* **2022**, *12*, 5773. [CrossRef]
8. Ranjha, M.M.A.N.; Kanwal, R.; Shafique, B.; Arshad, R.N.; Irfan, S.; Kieliszek, M.; Kowalczewski, P.L.; Irfan, M.; Khalid, M.Z.; Roobab, U.; et al. A critical review on pulsed electric field: A novel technology for the extraction of phytoconstituents. *Molecules* **2021**, *26*, 4893. [CrossRef] [PubMed]
9. Frelinger, A.L., 3rd; Gerrits, A.J.; Garner, A.L.; Torres, A.S.; Caiafa, A.; Morton, C.A.; Berny-Lang, M.A.; Carmichael, S.L.; Neculaes, V.B.; Michelson, A.D. Modification of pulsed electric field conditions results in distinct activation profiles of platelet-rich plasma. *PLoS ONE* **2016**, *11*, e0160933. [CrossRef] [PubMed]
10. Pavlin, M.; Kandušer, M.; Reberšek, M.; Pucihar, G.; Hart, F.X.; Magjarević, R.; Miklavčič, D. Effect of cell electroporation on the conductivity of a cell suspension. *Biophys. J.* **2005**, *88*, 4378–4390. [CrossRef] [PubMed]

11. Pavlin, M.; Leben, V.; Miklavcic, D. Electroporation in dense cell suspension: Theoretical and experimental analysis of ion diffusion and cell permeabilization. *Biochim. Biophys. Acta* **2007**, *1770*, 12–23. [CrossRef] [PubMed]
12. Canatella, P.J.; Karr, J.F.; Petros, J.A.; Prausnitz, M.R. Quantitative study of electroporation-mediated molecular uptake and cell viability. *Biophys. J.* **2001**, *80*, 755–764. [CrossRef] [PubMed]
13. Golberg, A.; Bei, M.; Sheridan, R.L.; Yarmush, M.L. Regeneration and control of human fibroblast cell density by intermittently delivered pulsed electric fields. *Biotechnol. Bioeng.* **2013**, *110*, 1759–1768. [CrossRef] [PubMed]
14. Redondo, L.M.; Silva, J.F. Repetitive high-voltage solid-state Marx modulator design for various load conditions. *IEEE Trans. Plasma Sci.* **2009**, *37*, 1632–1637. [CrossRef]
15. Ruiz-Fernández, A.R.; Campos, L.; Gutierrez-Maldonado, S.E.; Núñez, G.; Villanelo, F.; Perez-Acle, T. Nanosecond pulsed electric field (nsPEF): Opening the biotechnological Pandora's box. *Int. J. Mol. Sci.* **2022**, *23*, 6158. [CrossRef] [PubMed]
16. Atsu, P.M.; Mowen, C.; Thompson, G.L. Enhanced cell viability and migration of primary bovine annulus fibrosus cells with microsecond pulsed electric field exposure. *ACS Omega* **2023**, *8*, 36247–36258. [CrossRef] [PubMed]
17. Jordan, E.T.; Collins, M.; Terefe, J.; Ugozzoli, L.; Rubio, T. Optimizing electroporation conditions in primary and other difficult-to-transfect cells. *J. Biomol. Tech.* **2008**, *19*, 328–334. [PubMed]
18. Liao, F.; Li, Y.; Zhang, Z.; Yu, Q.; Liu, H. Pulsed electromagnetic fields modulate energy metabolism during wound healing process: An in vitro model study. *BMC Complement. Med. Ther.* **2025**, *25*, 50. [CrossRef] [PubMed]
19. Sherba, J.J.; Hogquist, S.; Lin, H.; Shan, J.W.; Shreiber, D.I.; Zahn, J.D. The effects of electroporation buffer composition on cell viability and electro-transfection efficiency. *Sci. Rep.* **2020**, *10*, 3196. [CrossRef] [PubMed]
20. Watanabe, Y.; Nihonyanagi, H.; Numano, R.; Shibata, T.; Takashima, K.; Kurita, H. Influence of electroporation medium on delivery of cell-impermeable small molecules by electrical short-circuiting via an aqueous droplet in dielectric oil: A comparison of different fluorescent tracers. *Sensors* **2022**, *22*, 2494. [CrossRef] [PubMed]
21. Eisenstein, M. Transfection of mammalian cells by electroporation. *Nat. Methods* **2006**, *3*, 67. [CrossRef]
22. Potter, H.; Heller, R. Transfection by electroporation. *Curr. Protoc. Mol. Biol.* **2003**, *62*, 9.3.1–9.3.12. [CrossRef] [PubMed]
23. Wije Munige, S.; Bhusal, D.; Peng, Z.; Chen, D.; Yang, Z. Developing a cell quenching method to facilitate single cell mass spectrometry metabolomics studies. *JACS Au* **2025**, *5*, 2379–2387. [CrossRef] [PubMed]
24. Wilkins, J.; Sakrikar, D.; Petterson, X.-M.; Lanza, I.R.; Trushina, E. A comprehensive protocol for multiplatform metabolomics analysis in patient-derived skin fibroblasts. *Metabolomics* **2019**, *15*, 83. [CrossRef] [PubMed]
25. Caldeira, V.; Fonseca, T.A.H.; N'Dembo, L.; Araújo, R.; Von Rekowski, C.P.; Sampaio, P.N.S.; Calado, C.R.C. A new methodology for a rapid and high-throughput comparison of molecular profiles and biological activity of phytoextracts. *Biotechnol. Bioeng.* **2024**, *121*, 3047–3058. [CrossRef] [PubMed]
26. Ramalhete, L.; Araújo, R.; Vieira, M.B.; Vigia, E.; Pena, A.; Carrelha, S.; Ferreira, A.; Calado, C.R.C. Rapid FTIR Spectral Fingerprinting of Kidney Allograft Perfusion Fluids Distinguishes DCD from DBD Donors: A Pilot Machine Learning Study. *Metabolites* **2025**, *15*, 702. [CrossRef] [PubMed]
27. Pasieczna-Patkowska, S.; Cichy, M.; Flieger, J. Application of Fourier Transform Infrared (FTIR) Spectroscopy in Characterization of Green Synthesized Nanoparticles. *Molecules* **2025**, *30*, 684. [CrossRef] [PubMed]
28. Pucihar, G.; Mir, L.M.; Miklavčič, D. The effect of high frequency electric pulses on cell membrane permeabilization and recuperation. *Biochim. Biophys. Acta (BBA)–Biomembr.* **2012**, *1818*, 1220–1228. [CrossRef] [PubMed]
29. Kotnik, T.; Rems, L.; Tarek, M.; Miklavčič, D. Electroporation-based applications in biotechnology. *Trends Biotechnol.* **2019**, *37*, 1185–1206. [CrossRef] [PubMed]
30. Raso, J.; Frey, W.; Ferrari, G.; Pataro, G.; Knorr, D.; Teissie, J.; Miklavčič, D. Recommendations guidelines on the key information to be reported in studies of application of PEF technology in food and biotechnological processes. *Innov. Food Sci. Emerg. Technol.* **2016**, *37*, 312–321. [CrossRef]
31. Jesus, A.R.; Duarte, A.R.C.; Paiva, A. Use of natural deep eutectic systems as new cryoprotectant agents in the vitrification of mammalian cells. *Sci. Rep.* **2022**, *12*, 8394. [CrossRef] [PubMed]
32. Shorokhova, M.A.; Pugovkina, N.A.; Zemelko, V.I.; Lyublinskaya, O.G.; Grinchuk, T. Long-term cryopreservation may cause genomic instability and the premature senescence of cells. *Int. J. Mol. Sci.* **2024**, *25*, 1467. [CrossRef] [PubMed]
33. Potočnik, T.; Miklavčič, D.; Maček Lebar, A. Effect of Electroporation and Recovery Medium pH on Cell Membrane Permeabilization, Cell Survival and Gene Transfer Efficiency In Vitro. *Bioelectrochemistry* **2019**, *130*, 107342. [CrossRef] [PubMed]
34. Rols, M.P.; Teissié, J. Electropermeabilization of mammalian cells. Quantitative analysis of the phenomenon. *Biophys. J.* **1990**, *58*, 1089–1098. [CrossRef] [PubMed]
35. Gaskin, D.J.; Katsumata, Y.; Ramachandran, T.K.; Pereira, A.M.; Shaw, B.A. Oxidative stress and the endothelium: Implications for cardiovascular cell biology. *Am. J. Physiol.–Cell Physiol.* **2009**, *296*, C1099–C1109. [CrossRef] [PubMed]
36. Gonciarz, W.; Lechowicz, Ł.; Urbaniak, M.; Kaca, W.; Chmiela, M. Use of Fourier-Transform Infrared Spectroscopy (FT-IR) for Monitoring Experimental Helicobacter pylori Infection and Related Inflammatory Response in Guinea Pig Model. *Int. J. Mol. Sci.* **2020**, *22*, 281. [CrossRef] [PubMed]

37. Rinnan, Å.; Van Der Berg, F.W.J.; Engelsen, S.B. Review of the most common preprocessing techniques for near infrared spectra. *Trends Anal. Chem.* **2009**, *28*, 1201–1222. [CrossRef]
38. Jolliffe, I.T.; Cadima, J. Principal component analysis: A review and recent developments. *Philos. Trans. R. Soc. A Math. Phys. Eng. Sci.* **2016**, *374*, 20150202. [CrossRef] [PubMed]

**Disclaimer/Publisher's Note:** The statements, opinions and data contained in all publications are solely those of the individual author(s) and contributor(s) and not of MDPI and/or the editor(s). MDPI and/or the editor(s) disclaim responsibility for any injury to people or property resulting from any ideas, methods, instructions or products referred to in the content.